J. Electroanal. Chem. **737** (2015) 218-225, doi: 10.1016/j.jelechem.2014.06.010

The interface between Au(100) and 1-butyl-3-methyl-imidazolium - bis(trifluoromethylsulfonyl)imide

Claus Müller, Soma Vesztergom[1], Tamás Pajkossy[2], Timo Jacob

Institute of Electrochemistry, University of Ulm, 89069 Ulm, Germany

Helmholtz-Institute-Ulm (HIU), Helmholtzstrasse, 89069 Ulm, Germany

Abstract

The electrochemical interface of Au(100) and an ionic liquid, $BMITf_2N$, has been characterized by cyclic voltammetry, electrochemical impedance spectroscopy and *in-situ* STM with the aim to compare this particular electrochemical system with the Au(100) | $BMIPF_6$ electrode. It is demonstrated that the two systems share the same electrochemical features: the capacitance spectra around the *pztc* show a double-arc structure on the complex plane, and the high frequency capacitance limits are practically the same in both systems. The double layer rearrangement processes are very slow; they proceed with time constants of minutes. Ordered adlayers of cations and anions have been imaged by *in-situ* STM.

Keywords: double layer, impedance, capacitance, potential of zero charge, *in-situ* STM, ionic liquid

1. Introduction

Ionic liquids (ILs) are defined as salts with melting points below 100 ^{o}C; many of them are fluid at room temperature. They have been attracting much interest recently in various areas of chemistry, both in academia and in the chemical industry, because of their beneficial properties like non-volatility, high ionic conductivity and nonflammability [1-4]. Ever since air- and water-stable imidazolium-based ILs have become known [5] and commercially available, ILs are expected to have a profound impact on electrochemistry [6,7]. From an electrochemical point of view, the most notable feature of ILs is their broad (4-5 volts wide) electrochemical stability window [8-12] which makes it possible to use them as electrolytes for the deposition of technical metals and other reactive materials [13-15].

Despite their great potential for new electrochemical applications, the interface structure and properties between a metal electrode and an IL is far from being well understood. This is

---

[1] Permanent address: Eötvös Loránd University, Pázmány Péter sétány 1/A, Budapest, Hungary, H-1117. Present address: Department of Chemistry and Biochemistry, University of Bern, Freiestraße 3, Bern, Switzerland, CH-3012.

2 Corresponding author. Permanent address: Institute of Materials and Environmental Chemistry, Research Centre for Natural Sciences, Hungarian Academy of Sciences, Magyar tudósok körútja 2, Budapest, Hungary, H-1117; e-mail: pajkossy.tamas@ttk.mta.hu

mainly due to the fact that most of the experimental studies were performed with polycrystalline − hence sometimes ill-defined − metal surfaces and/or with ILs of questionable purity. Therefore, the key points of doing double-layer studies in ILs are the use of single crystal surfaces with well-defined structures and clean ILs. This is why we have studied mostly Au single crystals in a commercially available high-purity imidazolium salt, 1-butyl-3-methyl-imidazolium-hexafluorophosphate ($BMIPF_6$) [16-19]. Apart from $BMIPF_6$, we made experiments also with a home-made guanidinium-based IL [20]; while the results reported in this paper were obtained with an ionic liquid comprising the same imidazolium-based cation as in $BMIPF_6$, but in combination with the bis(trifluoromethylsulfonyl)imide, Tf_2N^- anion (Figure 1). The first report on the double layer property measurements on $BMITf_2N$ have appeared just recently [21]. Unfortunately, this study was done not on Au, but on other electrode materials, Pt and carbon materials. Hence these results are not comparable with those of the present communication.

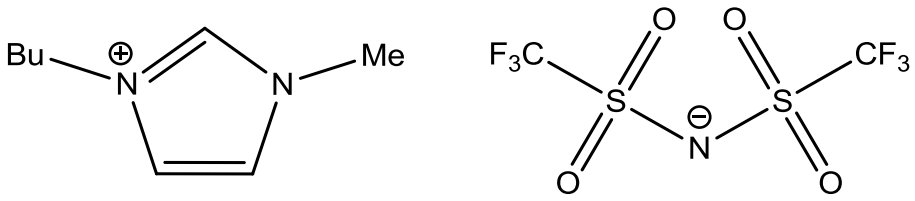

Fig. 1. Structure of 1-butyl-3-methyl-imidazolium-bis(trifluoromethylsulfonyl)imide, $BMITf_2N$.

The aim of the present study is two-fold: *i*.) to characterize the electrochemical interface between an Au(100) single crystal and the $BMITf_2N$ IL; and *ii*.) to make a comparison between this system and a very similar one, the previously studied Au(100) | $BMIPF_6$ electrode [17,18].

The main questions of the title subject are: what kinds of charge structures exist at the interface and how fast their rearrangement processes are. From this point of view, electrochemical impedance spectroscopy (a method to which Professor Tribollet has made considerable contributions [22]) plays a major role in this study.

The measurements presented here are very similar to those with $BMIPF_6$ summarized in reference [18]: basic characterization is done with cyclic voltammetry (CV); immersion measurements serve for the determination of the potential of zero total charge, *pztc*; electrochemical impedance spectroscopy (EIS) provides information regarding the double layer structure and relaxation processes therein. Finally, just as with $BMIPF_6$, *in-situ* scanning tunnelling microscopy (STM) images give a clue on the adlayer structure [23].

2. Experimental

2.1. Materials, electrochemical cells and basic electrochemical measurements

In general, the experimental conditions were similar to the ones described in references [18,20], only with different ILs. The experiments were carried out with the very same Au(100) single crystal of 12 mm diameter (MaTeck GmbH, Jülich, Germany) that was also used in [18,20]. $BMITf_2N$ was purchased from Merck KGaA in high quality (purity ≥ 99.5% , water ≤ 100 ppm, halides ≤ 100 ppm). The ionic liquid was vacuum-dried for 24 hours at elevated temperatures (80°C) and purified with a molecular sieve, as described in Ref. [19]. All experiments, including handling of the IL, were performed under nitrogen atmosphere, either in a glove box or in boxes with streaming nitrogen.

The CV and the EIS measurements were carried out in a cell made of Kel-F^{TM} with a volume of 0.3 cm^3; this is a cylindrical cell, the ends of which are the Au(100) working and a gold-sheet counter electrode; the reference electrode, a straight Ag wire coated with AgCl, is placed in-between and parallel to the electrodes (all potentials are quoted against the Ag/AgCl reference electrode). This construction ensured the strictly homogeneous current density distribution along the working electrode surface, which is an important condition for having reliable high-frequency impedance data with highly-resistive electrolytes.

Another cell of volume 0.2 cm^3 has been used for *in-situ* STM studies; since it is an open cell, it was also used for determining the potential of zero total charge (*pztc*) by immersing the electrode under potentiostatic control while recording and integrating the current transient.

2.2. Measurement and analysis of impedance spectra

Just as in the previous studies, we carried out EIS sequences with varied potentials, using a Zahner IM6 electrochemical impedance system controlled by the Thales Z 1.20 USB software. The EIS sequence was a cycle consisting of a step to the given potential, a typically one-hour delay, and finally a spectrum measurement with 5 mV amplitude between the limits of 1 MHz and 10 mHz. As a result, recording the spectra at 10 different potentials (just as it is shown in Figure 4) required about 20 hours measurement time. The two-hours-per-spectrum time appeared to be insufficient for stabilizing the system at a potential, as it was indicated by the distortion of the low frequency-end of the EIS-spectra . The bad data points (having a frequency always lower than 100 mHz) were identified by a Kramers–Kronig transform (in fact, a logarithmic Hilbert transform [24]), and were omitted from the curve fitting process.

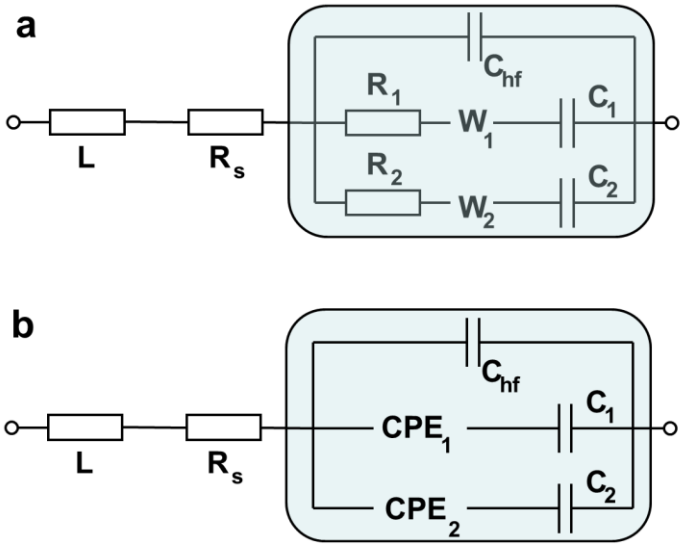

Fig. 2. Equivalent circuits used for fitting the spectra. The three-branched circuits in the boxes represent the interface. For the meaning of the individual elements see Sect. 2 (Experimental)

The reproducibility of the experiments could be well characterized by performing spectrum measurements at similar potentials at the beginning and end of the sequence. For example, the two lowermost spectra of Figure 4 were taken just as the first and the last terms of the sequence – with a time difference of about 20 hours – still, they are fairly similar to each other.

The impedance spectra were analyzed by fitting the parameters of appropriate equivalent circuits to the measured spectra by a non-linear least squares program using modulus weighting [25]. In other words, the fitting program minimized the sum of the $\left[(\mathrm{Re}Z_\mathrm{m} - \mathrm{Re}Z_\mathrm{c})^2 + (\mathrm{Im}Z_\mathrm{m} - \mathrm{Im}Z_\mathrm{c})^2\right] / \mathrm{Abs}Z_\mathrm{m}^{\,2}$ terms for all frequencies measured, where ReZ_m, ImZ_m, and AbsZ_m represent the real and imaginary components, and the absolute value of the measured impedance; ReZ_c and ImZ_c are the calculated real and imaginary components, respectively.

In double layer studies the best way to represent the results is to plot the capacitance spectra of the interface, $C(\omega)$ – calculated from the interfacial impedance $Z_i(\omega)$ as $C(\omega)=1/\left(i\omega Z_i(\omega)\right)$ – on the complex plane. In all our previous studies with ILs we came to the conclusion that the equivalent circuits shown in Figure 2 are appropriate to model *all* measured spectra: the three-branched part represents the interface (see later); R_s is the electrolyte resistance and L_s (of either sign, with $Z_{L_s} = i\omega L_s$) represents an error term; this element is a good approximation of the minor high frequency errors due to various imperfections of the measurement setup [26], mostly due to phase delays of the input amplifiers. The same applies for the present system, in case of which the $C(\omega)$ function appears on the complex plane as two arcs with a real, non-zero high frequency limit (C_hf). Regarding the analysis of the curves, the following comments are due here:

1. In case of some spectra, certain elements of the equivalent circuit were omitted from the fitting procedure, either because their values were too low (typically for R_2) or too high (typically for C_2). Were these elements included in the fitting, their error

would have been larger than their value, hence no accurate estimate can be assigned to the values of these elements. The quality of the fits were monitored by plotting the fitting residuals to identify systematic deviations of the fitted spectrum from the measured one, as it is shown in Fig.4b.

2. The W element of the circuit of Figure 2.a is a pseudo-Warburg impedance; that is, its frequency dependence $Z_W(\omega) \propto 1/\sqrt{i\omega}$ is the same as that of the impedance corresponding to planar diffusion. However, it must be emphasized that in our case W is merely an empirical term, and it cannot be related to any diffusion processes in the system. The constant phase elements incorporated in the model are, likewise, empirical terms.
3. The spectra of this study can well be fitted by the impedance function of both circuits of Figure 2; however, we preferred the use of the circuit in Figure 2a because of reasons detailed later in Section 3.2.

2.3. Immersion experiments

The flame-annealed Au(100) crystal was mounted in the empty STM cell, together with the reference and counter electrodes. All the electrodes were connected to the potentiostat and a certain potential was set. Subsequently the IL was injected by means of a pipette to quickly cover the whole electrode surface, assuring that the electrolyte first established contact with the reference and counter electrodes before hitting the working electrode. Although the wetting procedure required only less than 1 s, settling of the current is much slower, thus the current transients were recorded over several minutes.

2.4. STM

In-situ STM studies were performed with a Topometrix Discoverer TMX 2010 setup. For the preparation of the STM tips, Pt/Ir wires (80%/20%) were electrochemically etched in 3.5 M NaCN and coated with BASF electrophoretic paint to reduce the Faradaic current. Pt wires served as quasi-reference and counter electrodes. All images were recorded in the constant-current mode with 1 nA tip current. Before assembling the cells, the Au(100) single crystal was annealed in hydrogen flame for 10 min at yellow heat. and cooled down slowly in a nitrogen stream. After assembling the cell, the ionic liquid was filled into it by means of a pipette inside a glove box (MBRAUN LABstar) providing inert atmosphere.

3. Results and discussion

3.1 Cyclic voltammetry

Figure 3 shows the CV of an Au(100) electrode in contact with $BMITf_2N$. Significant cathodic and anodic faradic currents (>1 mA/cm^2) occur beyond −2 V and +2 V, respectively, thus the potential window of this IL is about 4 V. Just as in the case of $BMIPF_6$, passing the −2 V negative potential limit causes irreversible changes: the large cathodic current signals the reduction of the BMI^+ cation; a plausible mechanism suggests the generation of radicals that react with each other to form dimers [27]. Thus, we refrained from applying extreme (E < −0.8V and E>+0.8V) potentials: if the potential is kept or cycled in the middle of the potential window, then much smaller currents flow (see inset of Figure 3), however, in this potential range the CV and the impedance spectra are reproducible for many hours. The current here

is a charging current, the *dc* capacitance of the interface is $C_{dc} = j/v \approx 2\mu A/cm^2/50mV/s = 40\mu F/cm^2$. The **P** peak at E = −0.2V appears only when the scan direction is negative, while its anodic counterpart is broadened (it is a wave rather than a peak). As **P** is in the vicinity of the *pztc* (see below) its origin is most probably the anion/cation replacement at the surface. The **P** peak is located somewhat more negative than in case of Au(100) in $BMIPF_6$, but with approximately the same size and shape.

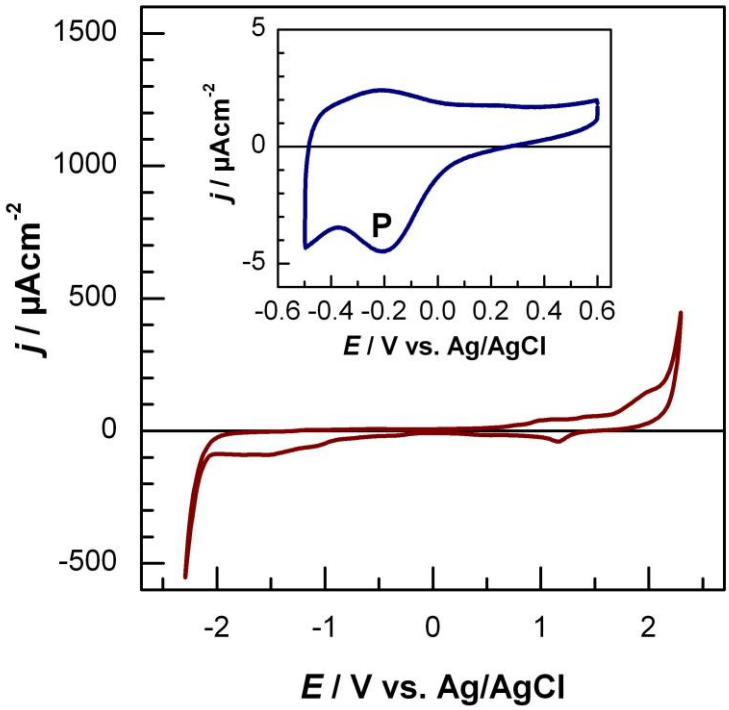

Fig. 3. CVs of v = 50 mV/s scanrate for the Au(100)|$BMITf_2N$ system between limits of $|j|$ < 0.5mA/cm^2**,** and in the middle of the potential window (inset).

3.2 Impedance spectra

Impedance spectra, $Z(\omega)$, have been measured within the −0.5V ≤ E ≤ +0.5V potential range as a function of potential. Just as in the case of Au(100)|$BMIPF_6$ [17], these spectra can be very well fitted (typically with $\chi^2 \approx 10^{-5}$) by the impedance function of the equivalent circuit shown in Figure 2-a. As it is displayed in Figure 4.b, the fitting residuals (deviation of the measured and fitted values) are smaller than 1% and 1 degree for each and every data point of all spectra. The interfacial term of the impedance is transformed to a capacitance representation using $C(\omega)=1/i\omega\left(Z(\omega)-R_s-i\omega L\right)$, where R_s is the series resistance and L the high-frequency correction term, both determined by fitting. For each potential the capacitance spectra show a two-arcs structure (as shown in Fig. 4a).

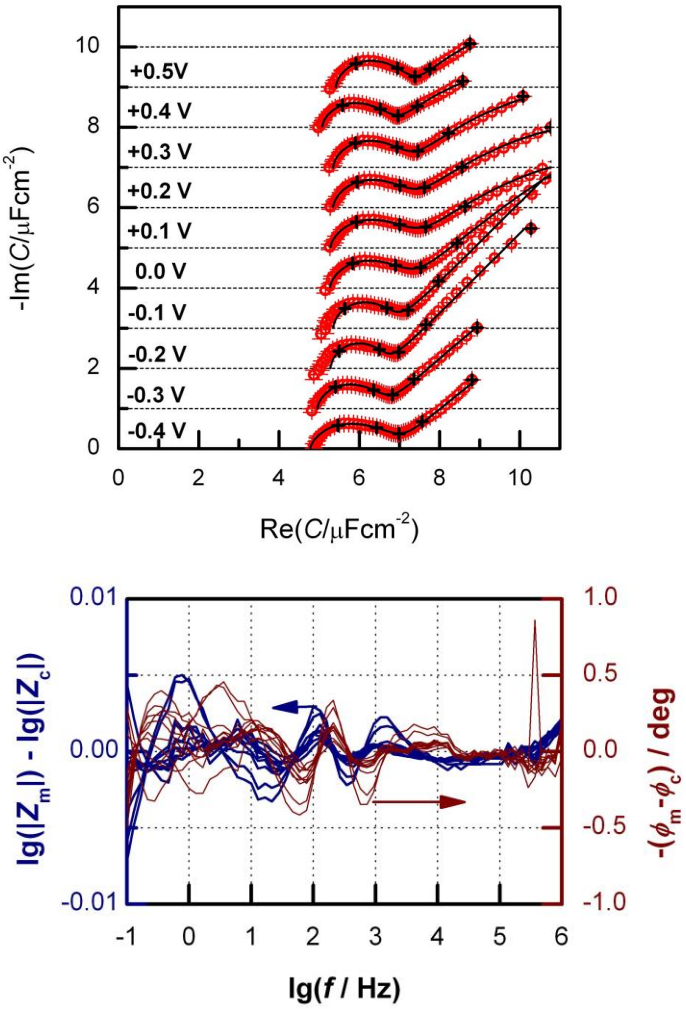

Fig. 4. (**a**): Complex plane plot of the capacitance spectra at potentials indicated. The 10^k Hz data points (between 10kHz and 0.1 Hz) are marked by crosses; solid lines are the fitted curves according to the equivalent circuit of Fig. 4a. The spectra are shifted along the ordinate for visibility reasons. (**b**) Differences of measured and fitted spectra of Fig. 3a. Thick and thin lines are for logarithmic magnitude and phase angle differences, respectively.

Three aspects are to be noted. First, the high-frequency limit of the capacitance is 4−5 μF/cm^2, practically independently of the potential. Second, the capacitances at low-frequencies are larger around −0.1V than elsewhere, which is in accordance with the appearance of the **P** hump in the corresponding CV. Third, the spectra can be well-fitted also by using the impedance function of the circuit shown in Figure 2.b, containing CPEs as used in a recent study on a similar system [26]. Both circuits of Figure 2 are empirical models; however, we prefer using the model shown in Figure 2.a as this is consistent with our previous studies on Au(100) in $BMIPF_6$ [18], and those spectra *cannot* be fitted by using the model of Figure 2.b. In both ILs the interfacial capacitance spectra are double-arcs in the complex plane, however, the high-frequency arc is much more pronounced for the present system, as it is shown at two potentials for the two systems in Figure 5. Reasons for the differences are not understood yet; all what can be safely stated is that the high-frequency capacitance is more-or-less the same for the two systems, ≈5 μF/cm^2.

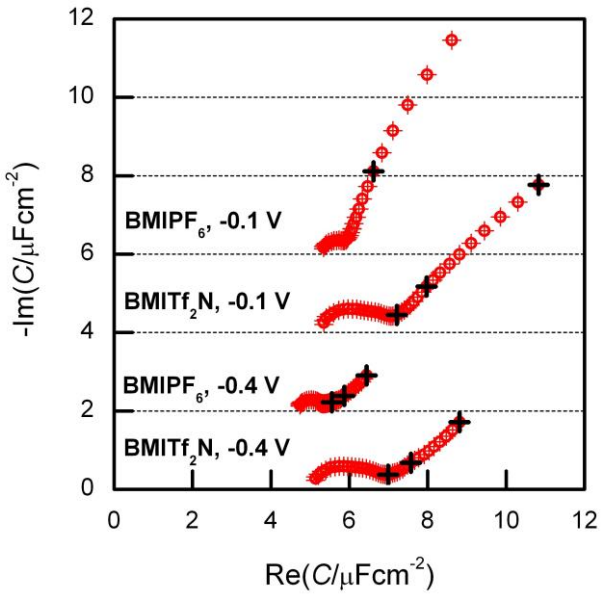

Fig. 5. Comparison of impedance spectra on Au(100) in $BMITf_2N$ and in $BMIPF_6$. The latter spectra are the ones of [18], Fig. 3. The 10Hz, 1 Hz and 0.1Hz data are marked by crosses.

Just as with Au(100) in $BMIPF_6$ [18] we attempted to identify the origin of the equivalent circuit elements of the impedance measurements. To this end we measured impedance spectra at varied temperatures, from room temperature up to 120 ^{o}C. Unfortunately, the thermal stability of this IL was not sufficient to obtain reproducible spectra during the heating and cooling procedures. Still, we found that the interfacial admittance increases with temperature – just as the bulk conductivity does – similarly to what is shown in Figure 7 of reference [18] and Figure 3.b of reference [20] for other Au(100) | IL systems. This finding is in accordance with the conclusions of reference [28] based on temperature-dependent EIS measurements on the Au(111) | $[Py_{1,4}][FAP]$[3] system.

3.3 Determination of the pztc

All but one current–potential–time measurement methods in electrochemistry provide information on charge changes of the electrodes rather than on the charge itself: this is the immersion measurement by which the actual electronic charge density of the electrode can be determined. By this method a clean (typically freshly prepared, bare) electrode is immersed into the electrolyte at a pre-set potential and the current density necessary for charging of the electric double layer is recorded [29,30,31]. These current transients are integrated yielding a charge density, which is then plotted versus the applied (immersion) potential.

[3] $[Py_{1,4}][FAP]$: 1-butyl-1-methylpyrrolidinium tris(pentafluoroethyl)trifluorophosphate

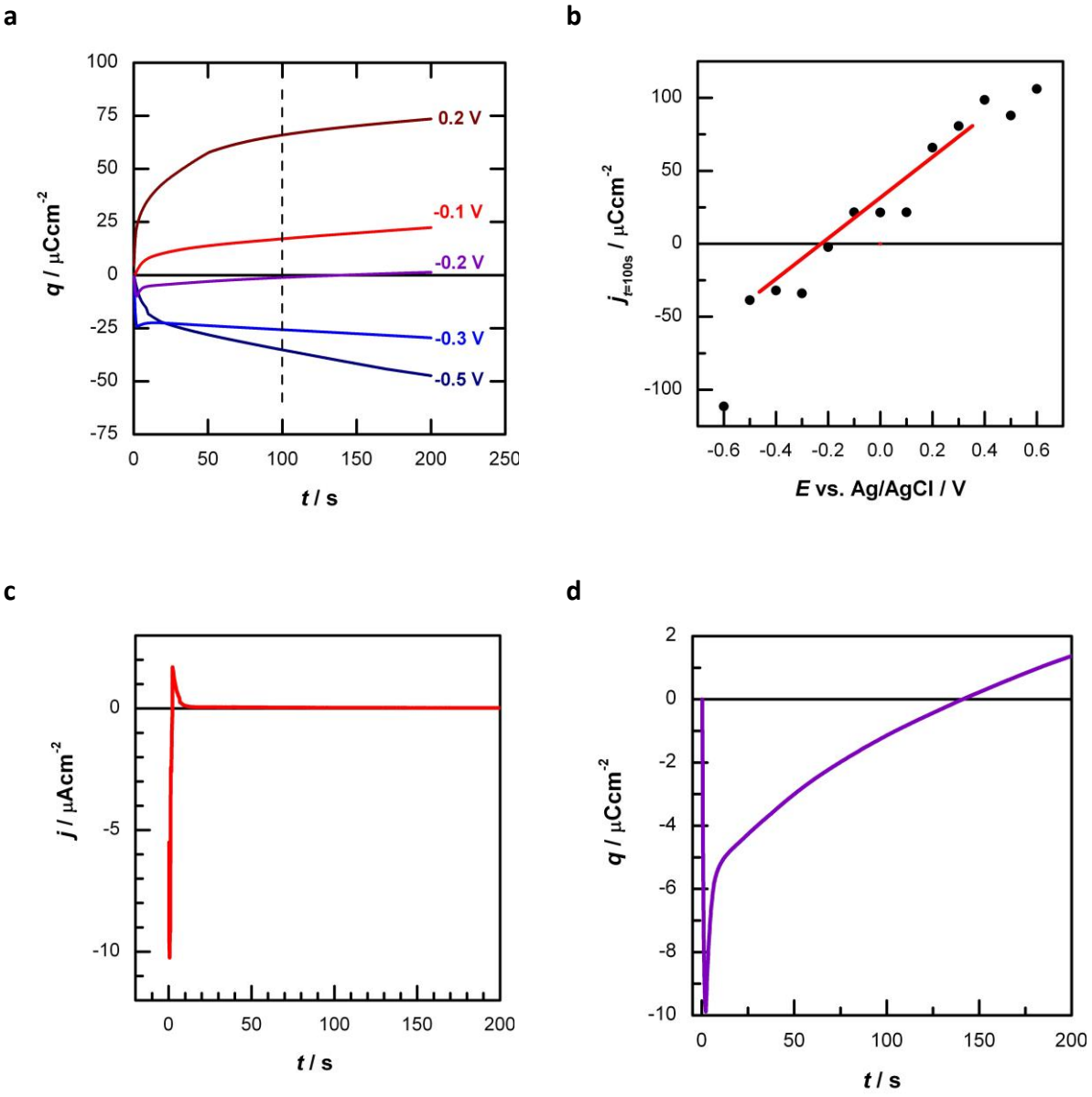

Fig. 6. (**a**): Integrated immersion transients at potentials indicated for Au(100) in $BMITf_2N$; (**b**): the charge calculated for 100 s as function of potential. The zero crossing is around -0.2 V, where the immersion current transient starts with a negative spike followed by a positive one (**c**) yielding that the surface charge initially negative and very slowly changes to positive (**d**).

The integrated current transients are shown in Figure 6.a. Unlike for the case of measurements in aqueous solutions [31] the charge-density curves do not converge to a final value, which means that the current transients follow a power-law rather than an exponential behaviour. Consequently, the charge depends on the duration of the experiment. To circumvent this, we calculated the charge at one and the same, arbitrarily chosen time, at 100 s. In Figure 6.b charges for 100 s integration time are plotted versus the immersion potential. The straight line marks the zero crossing, which is around −0.2V vs. Ag/AgCl, its slope corresponds to a value in the order of 150 μF/cm^2. The potential of the zero-crossing coincides with the cathodic peak **P** (cf. the inset of Fig. 3b). We presume that

this potential marks the rearrangement of the ionic liquid, when anions and cations exchange places as the potential is decreasing. Compared to Au(100) in $BMIPF_6$ the zero-crossing is shifted by about 50 mV towards more negative potentials [14].

3.4 In-situ STM studies

We found two potential ranges where STM imaging reveals structural details of the interface. First, anodic and cathodic to the *pztc* ordered adlayers of the anions and the cations can be imaged, respectively. Second, at sufficiently negative potentials the desorption of the cation adlayer can be observed along with the reconstruction of the Au(100) surface.

Positive to the *pztc* at +0.043V, Au(100) exhibits local restricted island, consisting of stripes with a thickness of approx. 2 nm and a distance of (2.5 ± 0.1) nm (Figure 7). Note that this distance is about one order of magnitude larger than the distance (0.29 nm) between two Au atoms. Two types of islands can be observed on the surface, the stripes of which have a perpendicular orientation to each other. As at this potential Tf_2N^- anions should be accumulated on the metal surface, the creation of these islands could be a hint of a fixed adlayer of Tf_2N^- on Au(100), and the direction of the stripes − in a not specified way − is related to the Au(100) lattice symmetry. With a molecule length of 0.9 nm [32], a double-row structure of Tf_2N^- is proposed within each strip. Figure 7.b also exhibits a noisy appearance of the surface next to the islands with slightly covered areas, which indicates that the formation of these adlayers is still in progress.

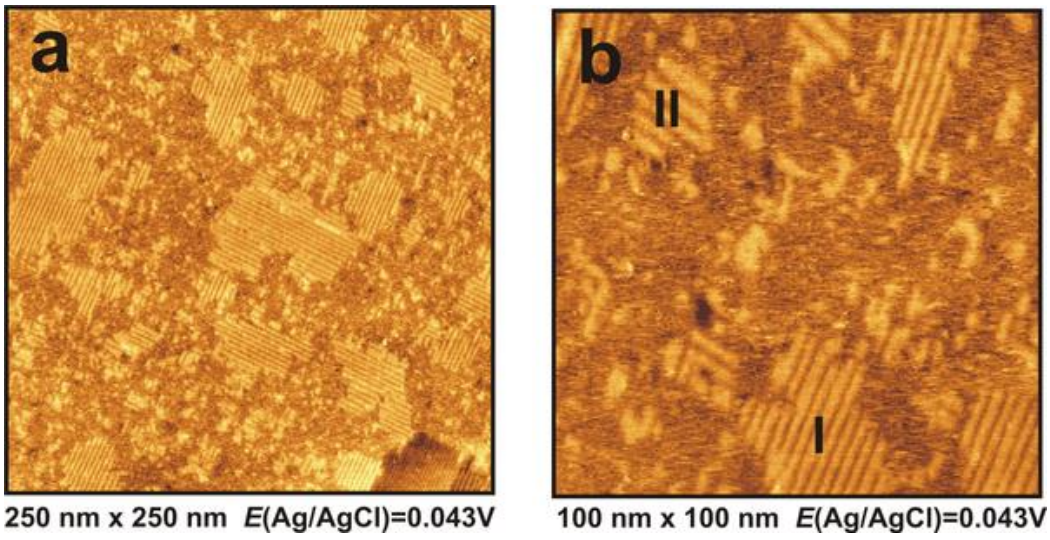

Fig. 7. STM images of the Au(100) surface. (**a**): Adsorption structure of Tf_2N^- at potentials positive of the *pztc*; (**b**): Stripes in a higher resolution.

For comparison, we note that the small BF_4^- anion forms an ordered $\begin{pmatrix} 3 & -1 \\ -1 & 3 \end{pmatrix}$ adlayer at positive potentials on Au(100) in contact with $BMIBF_4$ [23]. When the potential is set to values close to the *pztc* (−0.2V), the STM images become ill-defined und blurry (Figure 8). A possible explanation for this could be the fact, that at this potential neither the anions nor the cations should be dominant in the electrochemical interface. Therefore, a former fixed

adsorption structure of anions begins to loose and hence gains a higher mobility, which consequently reduces the quality of the STM images.

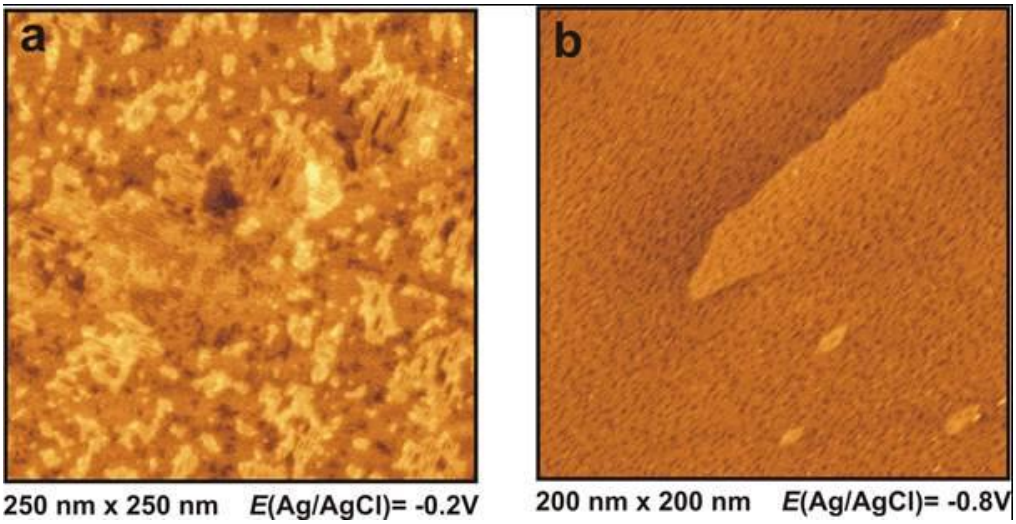

Fig. 8. STM images of the Au(100) surface. (**a**): Au(100) at a potential close to the *pztc* (−0.2 V); (**b):** Appearance of small holes in the surface presumably due to etching processes caused by BMI^+ at −0.8 V.

Negative to the *pztc*, at −0.8 V, the anion adlayer completely disappears. The image is comparable to the systems Au(100)|$BMIPF_6$ as well as Au(111)|$BMIBF_4$, a formation of small holes in the surface can be observed (Figure 8.b). The appearance of these surface defects was explained as a result of a reorganization of molecules within the IL layer in front of the electrode surface or as an onset of a cation-induced etching process, respectively [12,18,23].

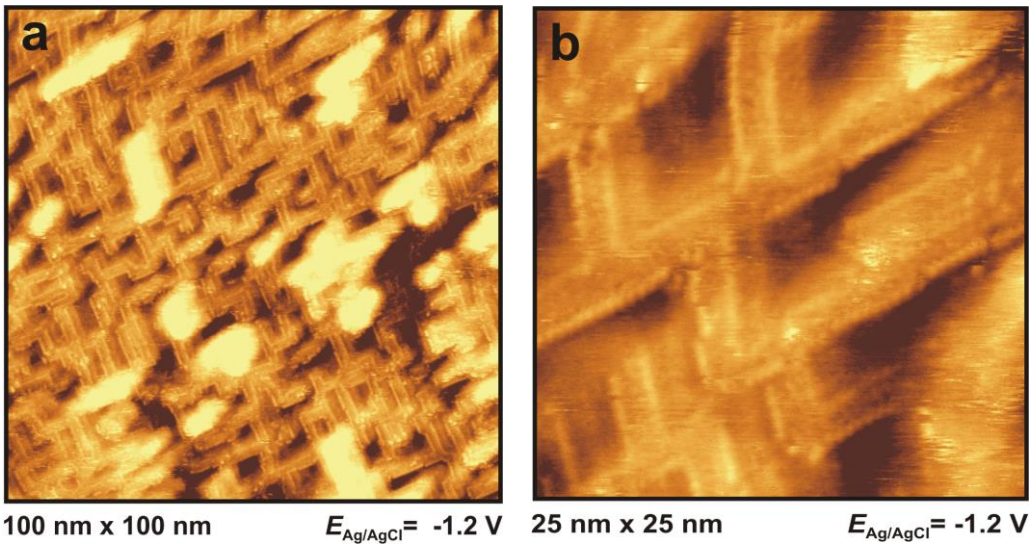

Fig. 9. STM images of the Au(100) surface. (**a**): Cation row structure of BMI^+; (**b**): High resolution STM image of the adlayer structure.

An ordered adlayer becomes apparent when the electrode is kept at a potential of −1.2 V for several hours (Figure 9.a). The four-fold symmetry of Au(100) acts as kind of a template for

BMI^+ cations, which are arranged in stripes of a rectangular pattern ("U"-shaped domains) [33].

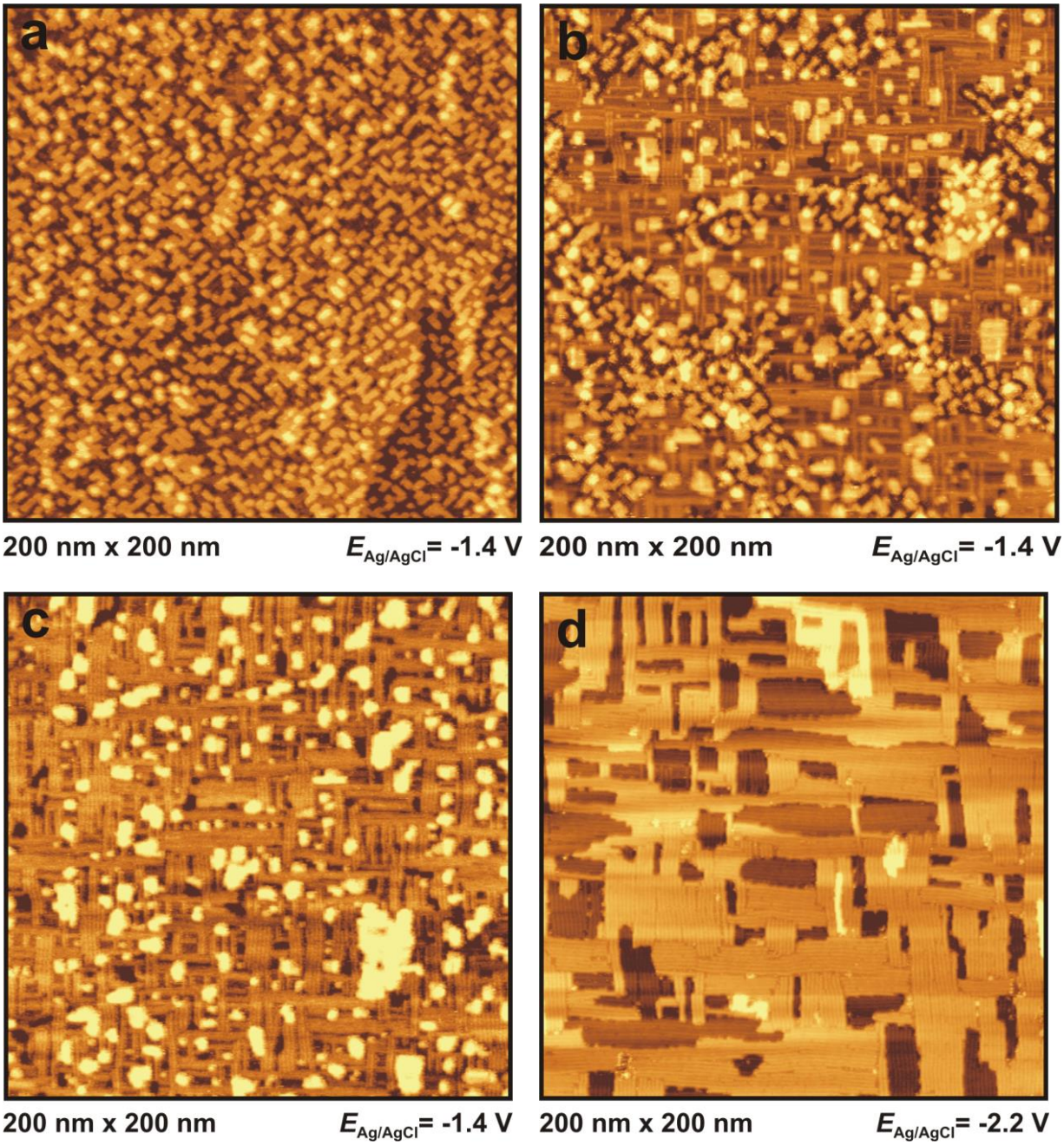

Fig. 10. STM images of the Au(100) surface. Series of STM images at −1.4 V (**a–c**): slow desorption of BMI^+ and formation of Au(100)-hex; (**d**): Completely potential-induced reconstruction at −2.2 V.

Figures 10.a−10.c exhibit a series of STM images taken at a potential of −1.4 V. The Au(100) surface, previously covered by a BMI^+ row-structure (Figure 9.a), starts to become unstable and a time-dependent process of cation desorption and a simultaneous formation of potential-induced hexagonal-reconstruction rows commences to take place. Hereof the following observation can be made: after 90 minutes, still existing adlayer domains as well as

already reconstructed parts of bare Au(100) can be distinguished at the surface. During the next 60 minutes this process advances, indicated by the fact that the adlayer domains get visualized as bright islands, which implies the onset of their desorption (Figure 10.c). Based on this observation we assume that the unreconstructed Au(100)-(1×1) surface is below the adsorbed cations.

Decreasing the potential to −2.2 V causes a complete disappearance of the last remains of adlayers. Since this potential corresponds to the cathodic limit of the CV, the decomposition of $BMITf_2N$ (*i.e.* cation breakdown) triggers strong reductive currents. Figure 10.d reveals an entirely reconstructed surface, which was also observed and described in detail for Au(100) in aqueous electrolytes [34,35].

4. Discussion

For the different Au(100) and Au(111) electrodes in contact with ILs containing BMI^+ and guanidinium-cations the double layer rearrangement processes appear to be very slow. This statement is based on "classical" electrochemical measurements, such as CV and EIS, as well as on the time-dependent changes in the corresponding STM images, showing that most of the ordered structures of Figures 7−10 are formed after a sufficiently long time (several minutes). The low-frequency limit value of the capacitance is not accessible by measurements, since it is at extremely low frequencies, below the mHz region. Hence steady state − the essential condition for accurate impedance measurements − does not exist. Instead, one has to determine the accessible frequency range by Kramers−Kronig transform.

The capacitance spectra exhibit two arcs and a real, non-zero, high-frequency limit value on the complex plane, even if for some of the spectra the downward bending part of the low-frequency arc is missing at the given frequency range of the measurement. Accordingly, the equivalent circuit of the interface consists of three capacitive branches, as shown in Figure 2. In the first branch, the single capacitive element is responsible for the high frequency limit of the capacitance. As shown in Figure 5, high-frequency limit of the capacitance is about 5 $\mu F/cm^2$ for both BMI-based ionic liquids. (For comparison, we note that in a guanidinium-based ionic liquid C_{hf} is as low as 1 $\mu F/cm^2$.) A plausible interpretation of C_{hf}: it is the geometric capacitance of a parallel plate condenser whose plates are separated by about one monolayer of ions. We see little if any difference in the C_{hf} values measured at potentials positive and negative to the *pztc* − probably because the anions and the cations of $BMITf_2N$ are approximately of the same size. This finding and the related theories [36,37] that predict peaks in the range of 10−20 $\mu F/cm^2$ at the *pztc* are at variance with the present results.

The other two branches represent the double layer rearrangement kinetics due to potential changes, and the concomitant charge changes. The R−W−C and CPE−C circuits are empirical models rather than visualization tools of well-defined physico-chemical models. For the present system, Au(100) | $BMITf_2N$, both circuits were applicable. Alternatively, the equivalent circuit of Figure 2.a was found to be appropriate for Au(100) | $BMIPF_6$ and Au(100) | $BMITf_2N$; the circuit of Figure 2.b was definitely inappropriate for Au(100)|$BMIPF_6$, but appropriate for Au(100)|$BMITf_2N$, Au(111)|$BMIPF_6$ [16], Au(100)|guanidinium-based ILs [20], and also for the Au(111)|[EMI][FAP][4] system [38]. The connection of the models and

[4] [EMI][FAP]: 1-ethyl-3-methylimidazolium tris(pentafluoroethyl)-trifluorophosphate

systems, just as the physical meaning of the W- and/or CPE-elements still remains an open issue. In addition it is unclear so far whether or not the two capacitive arcs can be coupled or related to the two ions of the ILs.

The interfacial capacitance is the larger the slower the potential perturbation is, as it is manifested in the strong frequency-dependence of the points of the capacitance spectra. Qualitatively, this can be observed if the capacitances are considered calculated from the CV and immersion charge measurements. These are about one order of magnitude larger than C_{hf} (≈5 μF/cm^2) in accord with the low potential perturbation rate (<<0.1Hz) of the latter measurements.

The STM images shown here clearly indicate ordered structures on the surface. Other physical methods also reveal ordering and layering. High-energy X-ray reflectivity studies exhibit the existence of a strong interfacial layering between ILs and charged sapphire electrodes [39]. This intense interaction was also revealed for Au(111) in contact with $BMPTf_2N$ in form of a 2D-liquid state adlayer by UHV-STM [32].

Atkin *et al.* and Zhang *et al.* detected several ionic-liquid layers in front of the electrode by measuring AFM force curves [40-42]. For the Au(111) | $BMIPF_6$ interface, the existence of interior and exterior layers next to the surface was reported. Here, the interior layers reveal a distinct reduced layer thickness and need a much stronger force to be ruptured [42]. This finding is in accordance with the observation of an (innermost) adlayer of BMI^+ regarding our electrochemical system. Figure 9.b exemplifies the constitution of the adsorption stripes. Its double-row structure of BMI^+ shows a close resemblance to our results and those of Mao's group concerning the electrochemical interface of Au(100)|$BMIPF_6$ [18,23,33].

Similar to this system, for Au(100)|$BMITf_2N$ it is also proposed that the imidazolium ring system is conform with the more intense outer spots of the double-row whereas the butyl chains are depicted by the murkier inner spots observed by *in-situ* STM. The width of each strip is (1.44 ± 0.15) nm. Unfortunately, it was not possible to obtain STM images in the same high quality as for $BMIPF_6$, but difficulties concerning STM studies were also reported for $EMITf_2N$ in combination with gold single crystals. The main reason for the reduced quality is attributed to a strong adsorption of Tf_2N^- even at negative potentials [33]. Reference [11] reports a breakdown of this kind of anion at higher negative potentials and an adsorption of its reduction products. However, these alleged decomposition currents could not be observed by using pure and dry ionic liquids [43]. Also for $BMITf_2N$, we assume a flat orientation of the BMI^+ cation layer, which is generated and stabilized by π–π interactions and van-der-Waals forces between the alkyl chains. Sum-frequency-generation-spectroscopy (SFG) measurements of the interface between imidazolium-based ILs and polycrystalline platinum confirm this presumption of a flat lying imidazolium ring at negative potentials [44,45].

5. Summary and conclusions

To characterize the interfacial properties of the Au(100) | $BMITf_2N$ system, electrochemical measurements were done and in-situ STM images were taken, with the following results:

By immersion experiments the *pztc* of the Au(100)|$BMITf_2N$ system has been determined to be at $E = -0.2$ V vs. Ag | AgCl. Positive and negative to the *pztc* ordered adlayers of anions and cations, respectively, exist, as have been revealed by STM images.

The CV and impedance behaviour of the Au(100)|$BMITf_2N$ system is similar to that of Au(100) | $BMIPF_6$. The capacitance spectra around the *pztc* are of double-arc shapes on the complex plane. The high-frequency capacitance limit is practically the same for the two systems. All changes at the interface associated with charging, observed by CV and impedance, and also adlayer dissolution, as imaged by *in-situ* STM, are very slow. Double layer rearrangements proceed with time constants of minutes rather than quasi-instantaneously as usually observed in aqueous solutions.

Acknowledgments

This cooperation was made possible by the exchange project of the Deutsche Akademische Austauschdienst and the Hungarian Fellowship Board, No. 39706. This study has been initiated by the late Professor D.M. Kolb in 2011. We acknowledge the contribution of Dr Markus Gnahm to some of the electrochemical measurements. Further, support by the Deutsche Forschungsgemeinschaft (DFG) through project KO 576/28-1 is gratefully acknowledged. S. Vesztergom gratefully acknowledges the financial support of the European Union, the State of Hungary and the European Social Fund given to his work in the framework of TÁMOP 4.2.4. A/11-1-2012-0001 'National Excellence Program'. S. Vesztergom further acknowledges the support of Scientific Exchange Programme NMS-CH (SciEx 13.060) for funding his internship at the University of Bern.

References

1 M. Freemantle, *Introduction to Ionic Liquids*, RSC Publishing, Cambridge, UK, 2009.

2 B. Kirchner (Ed.), *Ionic Liquids*, *Topics Curr. Chem.*, vol. 290, Springer, Heidelberg, Germany, 2010.

3 A. Kokorin (Ed.), *Ionic Liquids: Applications and Perspectives*, InTech, Rijeka, Croatia, 2011.

4 P. Wasserscheid, T. Welton, *Ionic Liquids in Synthesis*, Wiley-VCH, Weinheim, 2003.

5 J. S. Wilkes, M. J. Zaworotko, *J. Chem. Soc. Chem. Comm*. 1992, **13,** 965

6 F. Endres, S. Z. El Abedin, *Phys. Chem. Chem. Phys*. 8 (2006) 2101.

7 M. Galinski, A. Lewandowski, I. Stepniak, *Electrochim. Acta* 51 (2006) 5567

8 Y.C. Fu, Y.Z. Su, D.Y. Wu, J.W. Yan, Z.X. Xie, B.W. Mao, *J. Am. Chem. Soc*., 2009, **131**, 14728.

9 Y.-Z. Su, Y.-C. Fu, Y.-M. Wei, J.-W. Yan, B.-W. Mao, *ChemPhysChem*, 2010, **11**, 2764.

10 N. Borisenko, Z. El Abedin, F. Endres, *J. Phys. Chem. B*, 2006, **110**, 6250.

11 F. Endres, Z. El Abedin, N. Borissenko, *Z. Phys. Chem*., 2006, **220**, 1377.

12 L.G. Lin, Y. Wang, J.W. Yan, Y.Z. Yuan, J. Xiang, B.W. Mao, *Electrochem. Commun.*, 2003, **5**, 995.

13 F. Endres, *ChemPhysChem*., 2002, **3**, 144.

14 S.Z. El Abedin, M. Pölleth, S.A. Meiss, J. Janek, F. Endres, *Green Chem*., 2007, **9**, 549.

15 F. Endres, D. MacFarlane, A. Abbott, *Electrodeposition from Ionic Liquids*, Wiley-VCH, Weinheim, 2008.

16 M. Gnahm, T. Pajkossy, D.M. Kolb, *Electrochim. Acta,* 2010, **55,** 6212.

17 T. Pajkossy, D.M. Kolb, *Electrochem. Comm.,* 2011, **13,** 284

18 M. Gnahm, C. Müller, R. Répánszki , T. Pajkossy, and D.M. Kolb, *Phys.Chem. Chem. Phys*., 2011, **13,** 11627

19 M. Gnahm, D.M. Kolb, *J. Electroanal. Chem*., 2011, **651**, 250

20 M. Gnahm, C. Berger, M. Arkhipova , H. Kunkel, T. Pajkossy, G. Maas, and D.M. Kolb, *Phys.Chem.Chem.Phys*., 2012, **14**, 10647

21 C. Cannes, H. Cachet, C.Debiemme-Chouvy, C.Deslouis, J. de Sanoit, C. Le Naour, V.A.Zinovyeva, *J. Phys.Chem.C* 2013, **117**, 22915

22 M.E. Orazem, B. Tribollet, Electrochemical Impedance Spectroscopy, ISBN 978-0-470-04140-6, John Wiley, 2008

23 Y.-Z. Su, Y.-C. Fu, J.-W. Yan, Z.-B. Chen, B.-W. Mao, *Angew. Chem*., 2009, **121**, 5250.

24 W. Ehm, H. Göhr, R. Kaus, B. Roseler, C.A. Schiller, *ACH - Models in Chemistry,* 2000, **137**, 145

25 B.A. Boukamp, *Solid State Ionics* 1986, **18-19** 136

26 T. Pajkossy, *Electrochim. Acta,* 2010, **56,** 7246

27 M.C. Kroon, W. Buijs, C.J. Peters, G.-J. Witkamp, *Green Chem.*, 2006, **8**, 241.

28 M. Drüschler, N. Borisenko, J. Wallauer, C. Winter, B. Huber, F. Endres, B. Roling, *Phys. Chem. Chem. Phys*., 2012, **14**, 5090

29 V. Jendrašić, *J. Electroanal. Chem. Interfac. Electrochem*., 1969, **22**, 157

30 B. Jakuszewski, Z. Kozowoski, S. Partyka, M. Pszasnyski, S. Romanovski, *Soviet Electrochemistry,* 1971, **7**, 772

31 U.W. Hamm, D. Kramer, R.S. Zhai, D.M. Kolb, *J. Electroanal. Chem.*, 1996, **414**, 85.

32 B. Uhl, T. Cremer, M. Roos, F. Maier, H-P. Steinrück, J. Behm, *Phys.Chem.Chem.Phys*., 2013, **15**, 17295

33 Y.-Z. Su, J.-W. Yan, M.-G. Li, Z.-X. Xie, B.-W. Mao, Z.-Q. Tian, *Z.Phys.Chem*., 2012, **226**, 979

34 A.S. Dakkouri, D.M. Kolb, Reconstruction of gold surfaces, In: Interfacial electrochemistry: theory, experiment and applications, ed. A. Wieckowski, M. Dekker, New York, 151-173 (1999)

35 D.M. Kolb, *Angew. Chem*., 2001, **113**, 1198

36 A.A.Kornysev, *J.Phys.Chem.B*. 2007, **111,** 5545

37 K.B.Oldham, *J.Electroanal. Chem*., 2008, **613,** 131

38 M. Drüschler, B. Huber, B. Roling, *J. Phys. Chem. C*, 2011, 115, 6802

39 M. Mezger, H. Schröder, H. Reichert, S. Schramm. J.S. Okasinski, S. Schröder, V. Honkimäki, M. Deutsch B. M. Ocko, J. Ralston, M. Rohwerder, M. Stratmann, H. Dosch, *Science*, 2008, **322**, 424

40 R. Atkin, S. Zein El Abedin, R. Hayes, L.H.S. Gasparotto, N. Borisenko, F. Endres, *J. Phys. Chem*. C, 2009, **113**, 13266.

41 F. Endres, O. Höfft, N. Borisenko, L.H. Gasparotto, A. Prowald, R. Al-Salman, T. Carstens, R. Atkin, A. Bund, S. Zein El Abedin, *Phys. Chem. Chem. Phys*., 2010, **12**, 1724

42 X. Zhang, Y.-X. Zhong, J.-W. Yan, Y.-Z. Su, M. Zhang, B.-W. Mao, *Chem.Commun*., 2012, **48**, 582

43 S. Randström, M. Montanino, G. B. Appetecchi, C. Lagergren, A. Morenao, S. Passerini, *Electrochim. Acta*, 2008, **53**, 6397

44 S. Rivera-Rubero, S. Baldelli, *J. Phys. Chem*. B, 2004, **108**, 15133.

45 S. Baldelli, *Acc. Chem. Res*., 2008, **41**, 421